pH-Controlled Two-Step Uncoating of Influenza Virus

Sai Li,[†] Christian Sieben,[‡] Kai Ludwig,[§] Chris T. Höfer,[‡] Salvatore Chiantia,[‡] Andreas Herrmann,[‡*] Frederic Eghiaian,[†¶*] and Iwan A. T. Schaap[†¶]

[†]Drittes Physikalisches Institut, Georg-August-Universität, Göttingen, Germany; [‡]Institut für Biologie, AG Molekulare Biophysik, Humboldt-Universität zu Berlin, Berlin, Germany; [§]Institut für Chemie und Biochemie, Forschungszentrum für Elektronenmikroskopie, Freie Universität Berlin, Berlin, Germany; and [¶]Center for Nanoscale Microscopy and Molecular Physiology of the Brain (CNMPB), Göttingen, Germany

ABSTRACT Upon endocytosis in its cellular host, influenza A virus transits via early to late endosomes. To efficiently release its genome, the composite viral shell must undergo significant structural rearrangement, but the exact sequence of events leading to viral uncoating remains largely speculative. In addition, no change in viral structure has ever been identified at the level of early endosomes, raising a question about their role. We performed AFM indentation on single viruses in conjunction with cellular assays under conditions that mimicked gradual acidification from early to late endosomes. We found that the release of the influenza genome requires sequential exposure to the pH of both early and late endosomes, with each step corresponding to changes in the virus mechanical response. Step 1 (pH 7.5–6) involves a modification of both hemagglutinin and the viral lumen and is reversible, whereas Step 2 (pH $<$6.0) involves M1 dissociation and major hemagglutinin conformational changes and is irreversible. Bypassing the early-endosomal pH step or blocking the envelope proton channel M2 precludes proper genome release and efficient infection, illustrating the importance of viral lumen acidification during the early endosomal residence for influenza virus infection.

INTRODUCTION

A virus packs its genome in a protective, metastable shell, which also provides specificity for interaction with the host. For enveloped viruses, the viral shell is often a nested assembly of a capsid-like protein layer packed into a lipid bilayer. Viruses such as influenza A inherit their lipid envelope from the host cell membrane during budding, and after transmission to another host, that same envelope plays an important role in host recognition and viral entry. The envelope of the influenza virus is covered with spike glycoproteins, mostly hemagglutinin (HA), which permit virions to bind sialic acids at the plasma membrane (1), enabling their entry into the cell by endocytosis. Beneath the influenza lipid envelope, the M1 proteins form a quasi-continuous layer suggested to be organized in a helical fashion (2), presumably conferring the capsule/filament morphology observed for many influenza strains. M1 interacts with the eight viral ribonucleoprotein segments (vRNPs) that contain the viral genome. The rod-like vRNPs are arranged in a certain pattern within particles (one central RNP is surrounded by the remaining seven RNPs) (3).

To achieve delivery of the viral genome into the cytoplasm, vRNPs must disconnect from the M1 layer and the viral shell must open up to the cytoplasm via membrane fusion (1,4,5). All of these steps occur as the virus is ferried inside endosomal vesicles from the cell periphery to the perinuclear area. On their journey, virions undergo two distinct acidification steps, the first in early endosomes at pH ~5.5–6.0 and the second in late endosomes at pH ~5.0–5.5. Both steps have been found to be essential to influenza infection (6). Acidification of the viral lumen occurs in early endosomes as a consequence of the opening of the viral M2 proton channels at pH 6 (7). Although it is clear that genome release, membrane fusion, and M1 dissociation from the envelope occur at the pH of late endosomes, it has been suggested that the pH of early endosomes is sufficient to allow vRNP dissociation from the M1 layer (4,5). In addition, a recent report suggests that efficient release of vRNPs only takes place before significant dissociation of the M1 layer occurs (8). On the other hand, membrane fusion is impaired if the envelope is still tightly bound to the M1 layer (9). This indicates that vRNP release, M1 dissociation, and membrane fusion may be achieved not at once but rather through a step-by-step sequence regulated by the pH at early and late endosomes. However, there is no evidence so far that structural changes of the influenza virus occur at the pH of early endosomes.

Although the influenza virus possesses a conserved basic architecture, its heterogeneity prevents direct observation of how its building blocks dismantle on the way to genome release, using electron microscopy image reconstruction techniques. However, one expects that the gradual structural rearrangements of influenza virions at low pH translate into

Submitted August 13, 2013, and accepted for publication February 21, 2014.

*Correspondence: frederic.eghiaian@inserm.fr or andreas.herrmann@rz.hu-berlin.de

Sai Li and Christian Sieben contributed equally to this work.

Sai Li's present address is Oxford Particle Imaging Centre, Division of Structural Biology, Wellcome Trust Centre for Human Genetics, University of Oxford, Oxford OX3 7BN, United Kingdom.

Frederic Eghiaian's present address is U1006 INSERM, Aix-Marseille Universite, Parc Scientifique de Luminy, 13009 Marseille, France.

Editor: Levi Gheber.

0006-3495/14/04/1447/10 $2.00

http://dx.doi.org/10.1016/j.bpj.2014.02.018

measurable changes in the mechanical properties of individual viral particles. The method of choice for studying mechanical properties of viruses is atomic force microscopy (AFM). With AFM, the stiffness of single particles can be measured by indenting them with a nanometer-sized probe. This approach has previously been used to investigate the structure-function relationship of symmetrical protein shells (10–13). In a previous study, we demonstrated with AFM that the influenza virus stiffness is exceptionally low compared to that of all other viruses studied with AFM (14,15). This low stiffness is consistent with the noncontinuous organization of the M1 layer under the lipid envelope in the X-31 strain (16) and with the large variations in virus shape and size that originate from this lack of a well defined protein capsid.

To understand the mechanism of viral uncoating, we investigated the mechanics and fusion capabilities of the influenza A virus at different pH values corresponding to the luminal pH along the endosomal maturation pathway. Using AFM indentation experiments performed at these different pH values, we unraveled the contribution of viral spikes, M1, and the lipid bilayer to the viral mechanics, as well as the contribution of viral lumen components. In addition to the M1-related, irreversible softening of viruses at pH <5.5, we observed a reversible decrease in stiffness at pH 6.0 compared to neutral pH, showing that changes in the viral architecture had already occurred at that pH. We demonstrate the importance of this first step in bypass virus-cell fusion assays, in which genome release and nucleus infection by plasma-membrane-bound viruses is probed.

We provide evidence that the uncoating of the influenza virus starts in early endosomes and is completed in late endosomes, implying an excellent adaptation of the influenza A virus to the endosomal maturation pathway in mammalian cells. We discuss the various structural and regulatory mechanisms involved in this two-step unpacking of influenza, which will help us to understand the biological reasons for this peculiar feature.

MATERIALS AND METHODS

Sample preparation

Small unilamellar vesicles were prepared by extrusion, as described in our previous article (14). Influenza lipids were kept under nitrogen at all times. Influenza A/X-31 (H3N2) virus was propagated for 48 h in 11-day-old chicken eggs. The allantoic fluid was collected and cleared from cell debris by low-speed centrifugation at 3000 $\times$ g for 30 min. The virus was then pelleted by ultracentrifugation at 100,000 $\times$ g for 90 min. The virus pellet was resuspended in phosphate-buffered saline (PBS), pH 7.4, and homogenized with a Teflon-coated homogenizer. The total protein content was determined by BCS assay and the virus was stored in aliquots at -80°C. Influenza A/Panama/2007/99 was prepared in Madin-Darby canine kidney (MDCK) cells. Cells were infected at a ratio of 1:3 viruses/cell in Dulbecco's modified Eagle's medium (DMEM) supplemented with 0.2% bovine serum albumin (BSA) and 4 μg/mL TPCK trypsin. After 48 h, the virus was harvested as described above.

Removal of the HA ectodomain was performed by Bromelain digestion (17). To this end, 10 mg of the virus was incubated with 12.5 mg Bromelain (Sigma, St. Louis, MO) in Tris-EDTA buffer for 16 h at 37°C. The virus cores were pelleted by ultracentrifugation (100,000 $\times$ g for 2 h), washed in PBS, and stored at 4°C.

AFM and cantilevers

An MFP-3D microscope (Asylum Research, Santa Barbara, CA) and cantilevers (Olympus BL-RC150VB, spring constant $k_{cl} = 0.029 \pm 0.005$ N/m mean $\pm$ SD, $n = 264$, tip radius $\approx$ 30 nm) were used for all AFM experiments. Viruses were 200- to 400-fold diluted in PBS buffer, and 100 μL of the dilution was deposited on a glass microscope coverslip that was coated with a positively charged silane (3-[2-(2-aminoethylamino)ethylamino] propyltrimethoxysilane, Sigma) (18). Tests of alternative surface treatments did not result in a firm immobilization of the virus particles on the surface (Fig. S1 in the Supporting Material). The pH of the sample was adjusted by adding sodium citrate to PBS until the desired pH value was reached, and the virus stock (1 mg/mL) in PBS was 500$\times$ diluted in this buffer and kept at least 30 min at room temperature (RT) before AFM analysis. To test the reversibility of the incubation of viruses at low pH, viruses were first incubated in acidic buffers at 37°C for 20 min and brought back to pH 7 by dilution in large amounts of PBS. The particle stiffness was quantified by performing multiple indentation experiments on top of the particle. For each particle, four indentation curves were aligned and averaged. The averaged indentation curve was fitted between 100 and 200 pN with a linear function. This force mapping technique is described in detail in our previous article (14). To obtain the average stiffness for a 100 nm particle, we fitted the stiffness (k)-versus-height (d) plot to $k(d) = a/d$, where a is the fitting parameter. For the fit, only particles with a 45 to 150 nm height were used. Because the measured stiffness also depends on the shape of the particles, we excluded particles with an extended or flattened shape and included only approximately round particles in the analysis (Fig. S2).

Cryoelectron microscopy

Influenza A/X-31 stock was diluted in PBS with preadjusted pH, and incubated for 30 min. Sample droplets were applied to perforated (1 μm hole diameter) carbon-film-covered 200 mesh grids (R1/4 batch of Quantifoil, MicroTools, Jena, Germany), which had been hydrophilized before use by 60 s of plasma treatment at 8 W in a Baltec Med 020 device. The supernatant fluid was removed with a filter paper until an ultrathin layer of the sample solution was obtained that spanned the holes of the carbon film. The samples were immediately vitrified by immersing the grids into liquid ethane at its freezing point (90 K) using a guillotine-like plunging device. The vitrified samples were subsequently transferred under liquid nitrogen into a Philips CM12 transmission electron microscope (FEI, Hillsboro, OR) using a Gatan (Gatan, Pleasanton, CA) cryo-holder and stage (model 626). Microscopy was carried out at a 94 K sample temperature using the low-dose protocol of the microscope at a primary magnification of 58,300 and an accelerating voltage of 100 kV (LaB6-illumination). The defocus was set to 1.2 μm.

Acid-mediated bypass and immunostaining

MDCK cells were seeded in 12-well plates on 15 mm glass coverslips one day before the experiment. Influenza A/Panama/2007/99 (H3N2) was diluted in PBS to a concentration of 50 μg/mL. The virus was preincubated in PBS at the indicated pH with or without 10 μM amantadine. The cells were washed in PBS and the virus was added and incubated for 10 min on ice. Afterward, the cells were washed and virus fusion with the plasma membrane was triggered by adding fusion buffer (10 mM Hepes and 10 mM MES in PBS, pH 5) at 37°C for 5 min. The cells were washed again and

incubated in DMEM for another 30 min at 37°C. Subsequently, the cells were washed three times in PBS and fixed (2% paraformaldehyde and 0.02% glutaraldehyde in PBS) for 30 min at RT. The cells were washed twice in PBS and permeabilized for 20–25 min with PBS containing 0.5% Triton X-100 and 0.2% BSA. Primary antibodies against viral M1 (Virostat, Portland, ME) and NP-FITC (Millipore, Billerica, MA) were diluted 1:1000 in PBS supplemented with 0.2% BSA and the cells were labeled for 1 h. The cells were washed in PBS three times for 10 min each time and incubated with the secondary antibody (anti-goat Cy3, Sigma) for 1 h. The cells were counterstained with DAPI at a final concentration of 0.2 μg/ml and finally washed three times for 10 min each time. Samples were fixed using Mowiol (Roth, Salem, OR) and stored in the dark after drying at 4°C.

Infection efficiency analysis of influenza A virus in MDCK cells

The infection efficiency of influenza A virus was investigated in MDCK cells after acid bypass and compared with normal endocytotic infection. To this end, MDCK cells were seeded in 12-well plates on 15 mm glass coverslips one day before the experiment. For acid bybass, viruses were treated as described above. Acid bypass was conducted in the presence of 200 nM bafilomycin A. After washing, the cells were incubated in infection medium (DMEM, 0.2% bovine serum, and 200 nM bafilomycin A) for 5 h, fixed, and immunostained as described above. Images were taken using an Olympus FV1000 confocal microscope. Nuclear NP staining was analyzed using CellProfiler (19). Briefly, a macro (CellProfiler pipeline) was constructed as follows. First, images were loaded and nuclei were identified based on the DAPI stain. The NP signal was analyzed within the DAPI-identified nuclei and the results were stored in a newly generated database. The database was loaded into CellProfiler Analyst and the internal classifier was used to generate an image training set and to classify cells as infected or not infected based on the NP signal.

RESULTS

Influenza virions are mechanically distinct from liposomes

In two previous studies we showed, by AFM indentation experiments, that A/X-31 influenza viruses are slightly but significantly stiffer than what we measured for liposomes made out of viral lipids (14,15). In these studies, the integrity of the influenza virus was confirmed by comparing the height distribution of the AFM data with the size distribution obtained from electron microscopy and dynamic light-scattering experiments. The size distribution of the samples tested for the experiments described here was again identical (Fig. S3), which confirms that our samples are minimally affected by the AFM testing procedure. Disruption of the sample could only be achieved by drying and rehydration of the sample (Fig. S4; see also Carrasco et al. (20)).

The viral genome, proteins, and particularly the M1 layer are responsible for the difference in stiffness between the liposomes and the influenza viruses. From a mechanical standpoint, the M1 layer and the viral lipid bilayer can be considered as two springs connected in parallel. Thus, weakening of either the M1 layer or the envelope will lead to a reduction in the stiffness of the viral shell. Since the previous experiments were performed on two different instruments and on different sample preparations, we repeated the measurements on a larger number of samples to test how accurately we can quantify the contribution of the viral proteins and genome to its mechanical response. The stiffness of 92 influenza viruses (A/X-31 H3N2 strain) and 101 liposomes made out of viral lipids (from A/Japan/305/57 H2N2 strain) was measured by performing AFM indentation measurements on single particles (Fig. 1, *A* and *C*). Notably, single virus particles could be identified by AFM, as compared to electron microscopy (Fig. 1, *A* and *B*). A clear correlation between the height of the particles (here defined as their diameter, d) and the measured stiffness (k) was observed (Fig. 1 *D*): Since a scaling of $k \approx 1/d$ is expected for spherical shells (12), we fitted all data points with a reciprocal function (see Methods). This allows us to determine the average stiffness at $d = 100$ nm, which was 0.0274 ± 0.0009 N/m for viruses (mean ± SE; Table 1 (*pH 7.4*) and Fig. 1 *D*). This value is comparable with that reported earlier on a different isolate and AFM (15). The average liposome stiffness was 0.0196 ± 0.0004 N/m (Fig. 1 *D* and Table 1 (*pH 7.4*)). This value is almost identical with the value of 0.021 ± 0.001 N/m that we reported previously for lipids from a different virus strain (14). The average stiffness of the viral liposomes was 72% of that of viruses at pH 7.4. The scattering of the data, which originates from measurement errors and sample heterogeneity, makes it difficult to blindly attribute one single measurement to a given particle type (virus or liposome). However, if enough particles are measured, in our case ~100 of each species, the standard error of the mean is reduced, so that the statistical probability that both species belong to the same population becomes extremely small ($p = 1 \times 10^{-16}$, Table S1). We can therefore accurately distinguish the influenza virus from the viral liposomes based on their stiffness difference. The contribution of additional viral building blocks (spike proteins, M1, and vRNP) to that difference can now be systematically analyzed.

Spikes and viral core soften between pH 7.4 and 6.0

In addition to the M1 layer, viral spike glycoproteins also contribute to the measured stiffness. The spikes, consisting of HA and neuraminidase (NA), form an additional soft layer between the AFM tip and the viral shell (and also between the shell and the supporting surface). Mechanically speaking, the spike layer can be considered as a spring (k_{spike}) that is placed in series with the viral shell (k_{shell}), and the total spring constant (k_{total}) should decrease in the presence of spikes ($1/k_{total} = 1/k_{spike} + 1/k_{shell}$). To be able to separate the contribution from M1 and the viral spikes, we removed the latter's ectodomain by Bromelain digestion (17), which generates bald viruses (Fig. S5, *A* and *B*). Samples with and without spikes were tested by AFM at four different pH values

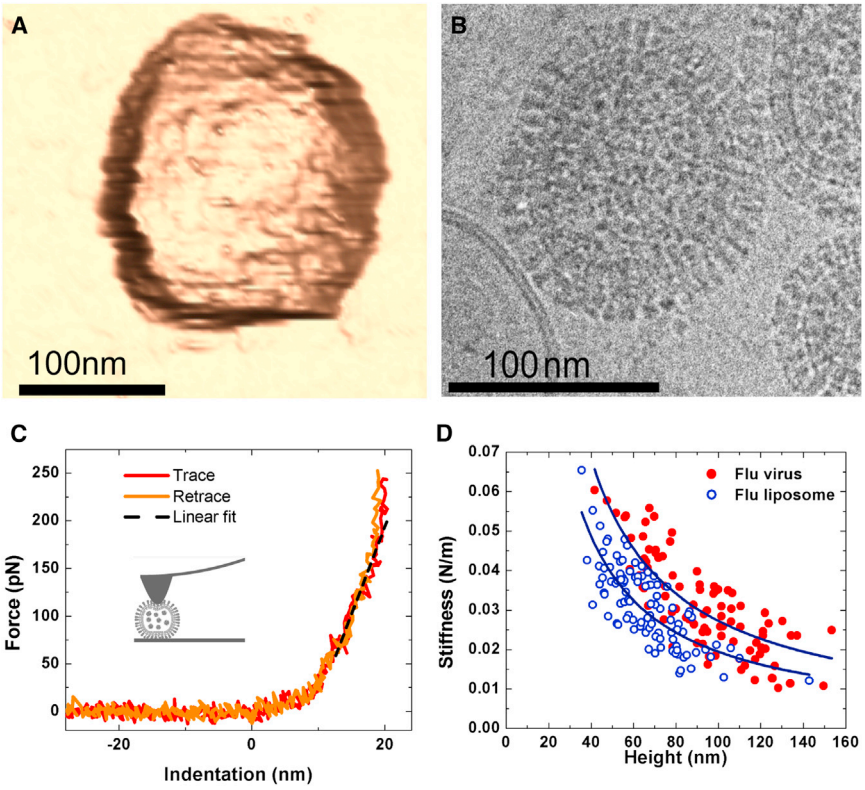

FIGURE 1 Influenza viruses are stiffer than liposomes. (*A*) Three-dimensional rendered image of an AFM topograph of an influenza A/X-31 virion adsorbed to a coverslip that was functionalized with a positively charged aminosilane in PBS at pH 7.4. (*B*) Cryo-electron micrograph of an influenza A/X-31 virion in PBS at pH 7.4. (*C*) Average force-versus-indentation curve collected on top of an X-31 influenza virion (measured height, 100 nm). Trace (i.e., tip pushes (*red*)) and retrace (i.e., tip retracts (*orange*)) are superimposed, indicating an elastic deformation regime. (*D*) Stiffness-versus-height plot of influenza A/X-31 viruses (*red*) and liposomes made from influenza viral lipids (*blue*). To see this figure in color, go online.

(7.4, 6.0, 5.5, and 5.0). At all pH values, bald viruses showed a higher stiffness than did intact viruses (Fig. 2 *A*). This confirmed that the decoration of the A/X-31 influenza virus by a soft layer of spikes reduces its total spring constant. This padding effect explains the counterintuitive observation that an intact virus at pH 5 appears even softer than a simple liposome. Comparing the stiffness-versus-pH curves of untreated and bald viruses the effective stiffness of the spikes at the different pH values can be calculated. Interestingly, the effective spring constant of the spikes was not constant but decreased at lower pH values (Fig. 2 *A*). This indicates that the spikes softened between pH 7.4 and 6.0 and remained soft when the pH was further lowered.

At first glance, it is tempting to attribute the observed softening to the pH-induced conformational change of HA, which represents ~85% of all spikes at the surface of the X-31 strain (16). However, the conformational change of HA, as well as HA-mediated fusion, occurs between pH 6.0 and 5.0 (Figs. S5 *C* and 2 *B*), which is in full agreement with other studies of the HA conformation and fusion activity (1,21,22). Therefore, the apparent softening of the spikes observed between pH 7.4 and 6.0 cannot be attributed to the fusogenic conformational change of HA. Instead, it could be explained either by an increase in spike mobility over the virus surface or by an increase in the flexibility of the spikes. In a study by Remeta and co-workers (22), it was shown that when the pH is lowered to 6, the denaturing temperature of HA is already considerably decreased, indicating a reduced stability. Artifacts related to a potential change of ionization of the virus and bald virus surfaces, resulting in

TABLE 1 Summary of AFM indentation measurements

pH	7.4	6.0	5.5	5.0	6.0 → 7	5.5 → 7	5.0 → 7
A/X-31 virus	0.0274 ± 0.0009 ($n = 90$)	0.0203 ± 0.0007 ($n = 102$)	0.0174 ± 0.0004 ($n = 101$)	0.0170 ± 0.0004 ($n = 106$)	—	—	0.0171 ± 0.0005 ($n = 79$)
Bald A/X-31 virus	0.0287 ± 0.0010 ($n = 89$)	0.0251 ± 0.0012 ($n = 72$)	0.0214 ± 0.0008 ($n = 68$)	0.0214 ± 0.0006 ($n = 90$)	0.0281 ± 0.0012 ($n = 74$)	0.0209 ± 0.0009 ($n = 67$)	0.0224 ± 0.0011 ($n = 78$)
A/Japan liposome	0.0196 ± 0.0004 ($n = 94$)	—	—	0.0187 ± 0.0006 ($n = 65$)	—	—	0.0170 ± 0.0005 ($n = 82$)

All measurements of particles (viruses and liposomes) with heights between 45 and 150 nm are reported here. In total, we measured 1257 single particles. An average of four indentation curves per particle was used to quantify their stiffness. To obtain the average stiffness for a 100 nm diameter particle we fitted each data set to $k(d) = a/d$, where k is the stiffness, d the diameter, and a a fit parameter. The standard deviation was obtained by a Gaussian fit of the distribution of residuals. This standard deviation was divided by the square root of the number of observations to give the mean ± SE values shown here.

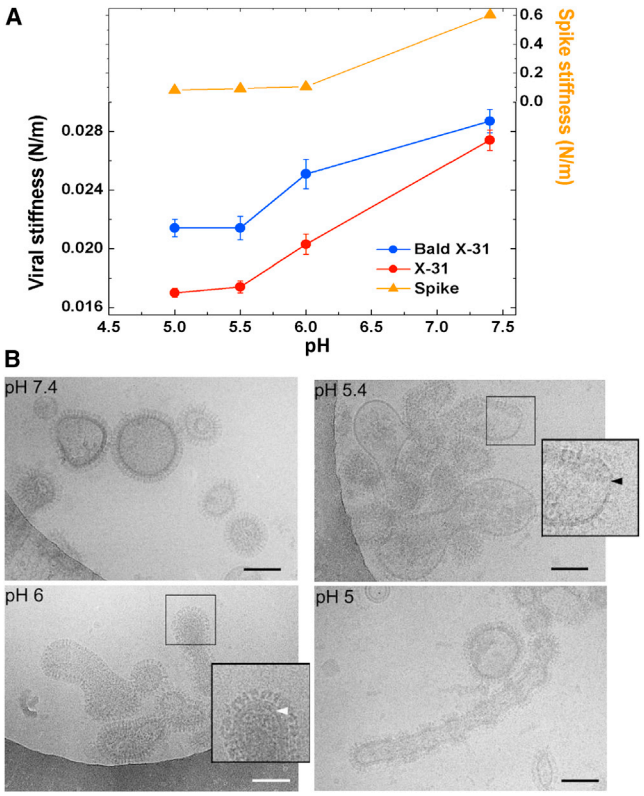

FIGURE 2 The apparent softening of the spikes is unrelated to the conformational change of HA. (*A*) Average stiffness of 100 nm bald viruses (*blue*) and untreated viruses (*red*) at different pH values. The stiffness of the spikes (*orange*) is obtained from the difference between the curves. (*B*) Cryoelectron micrographs of influenza A/X-31 viruses imaged after preincubation for 30 min at pH 7.4, 6.0, 5.4, or 5.0. An intact M1 protein layer is clearly visible in virions at pH 7.4 as well as at pH 6.0 (*white arrowhead*). In contrast, incubation at pH 5.4 led to a partial disassembly of M1 (*black arrowhead*) and a full collapse at pH 5.0. Scale bars, 100 nm. To see this figure in color, go online.

a pH-dependent surface attachment or tip-sample interaction, are unlikely to occur in our conditions (Fig. S6).

Notably, bald viruses also showed a small but significant reduction in stiffness in the range pH 7.4–6.0 ($p = 0.02$). This change must originate from a structural change in the viral core itself, probably as a result of the opening of the M2 proton channel and viral lumen acidification.

The M1 layer disassembles between pH 6.0 and 5.5

Intact and bald viruses showed a significant reduction in stiffness when the pH was lowered from 7.4 to 5.5. To verify that this effect is not due to the lipid bilayer itself, we repeated the experiments on liposomes formed from viral lipids. Their stiffness remained almost identical at all tested pH values (Table 1), from which we conclude that the lipid bilayer does not contribute to the pH effect on viral stiffness.

The strongest stiffness decrease of the virus took place between pH 6.0 and 5.5 (Fig. 2 *A*). The contribution of the spikes in that range is constant (see above); hence, it is most likely that this stiffness decrease signals the disassembly of the M1 layer. To verify this, we collected electron microscopy images from the viruses at the different pH values. Although the M1 layer was present at pH 7.4 and 6.0, we could not resolve it anymore at pH 5.4 and 5.0 (Fig. 2 *B*). Combined with our mechanical measurements, this shows that the disassembly of the M1 layer takes place between pH 6.0 and 5.5. Limited proteolysis of purified M1 confirmed our observations of a structural change within M1 after low pH incubation (Fig. S7). This observation is not fully consistent with other reports showing an intact M1 layer after 5 min incubation at pH 5.5 (23) and a sometimes incomplete dissociation of M1 after 5 min incubation at pH 4.9 (2). This discrepancy is likely explained by the longer exposure to acidic pH (30 min) in our conditions. However, in our earlier AFM report of influenza stiffness at pH 5.0, we report the same result despite a shorter incubation time (5 min), indicating that both partial and complete dissociation of M1 will lead to comparable virus softening (15).

Reversibility of the pH-dependent mechanical response

To test whether the changes within the virus are reversible, we analyzed the stiffness of viruses incubated at low pH and brought back to pH 7.4. Fig. 3 shows the reversibility results for bald viruses. The softening observed when the pH was lowered to 6.0 was largely reversed when the pH was brought back to 7.4. Since the ectodomains of the spikes were removed for these experiments, this reversibility of softening signals a change in the viral core. However, electron microscopy failed to show any M1 dissociation at this pH (Fig. 2 *B*), so other viral components must be involved in this reversible process. When the pH was lowered to

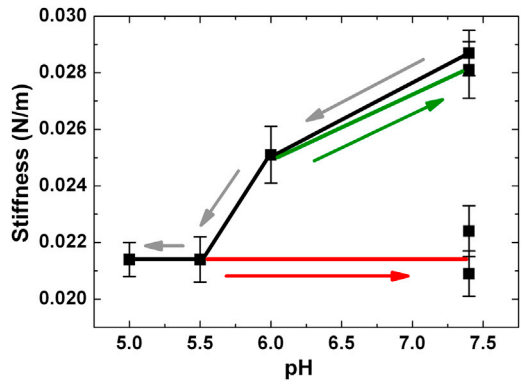

FIGURE 3 Reversibility of the pH-induced M1 disassembly. The stiffness of 100 nm bald viruses decreased with pH (*black line* and *gray arrows*). After neutralizing the buffer from pH 6.0 to pH 7.4, the stiffness recovers (*green line and arrow*). However, after neutralizing the buffer from pH 5.0 or pH 5.5 to pH 7.4, the stiffness does not recover (*red line and arrow*). To see this figure in color, go online.

5.5 or less and then brought back to 7.4, the viral stiffness remained as low as before neutralization (Fig. 3). Since we observed M1 dissociation at pH 5.5 and 5.0 (Fig. 2 *B*), our measurements indicate that the disassembly of the M1 layer is an irreversible process.

Subacidic pH is required for efficient vRNP release

So far, we have found two distinctive pH-induced phases of viral softening. In the first step, from pH 7.4 to pH 6.0, the stiffness of the spikes decreases, and we measured a small, reversible reduction in the stiffness of the viral core itself. In the second step, from pH 6.0 to pH 5.5, the M1 layer disassembles irreversibly.

Since the two above-mentioned pH regions correspond to those encountered in early and late endosomes, respectively, it seemed important to assess how relevant those conditions are to viral infection. We achieved this by performing acid bypass experiments (24). In this assay, by flushing the sample with a low-pH (5.0) buffer, fusion between the virus and the plasma membrane was triggered directly after cell adsorption of the virus. This procedure avoids a prolonged exposure of the virus to intermediate pH (6.0–7.4), since fusion with the plasma membrane simulates incubation of the virus in late-endosomal compartments with no prior transit through early endosomes.

For an efficient infection, vRNPs must separate from the remaining viral core and travel into the nucleus. To investigate the localization of M1 and NP after acid bypass, both proteins were marked by immunostaining and visualized by confocal microscopy. Notably, both proteins were localized inside the cytoplasm after acid bypass (Figs. S8 and S9). Fig. 4 *A* shows the cellular signals of M1 (*red*) and NP (*green*). When fusion was immediately triggered, i.e., by a pH jump at the plasma membrane, M1 and NP clustered and largely colocalized in the cytoplasm. When the virus was next preincubated at pH 6.0 for 30 min before fusion, to simulate transit of viruses through early endosomes, M1 and NP were still to some extent colocalized, but with fewer clusters, leading to an increase of the cytosolic signal for both proteins. Hence, a preincubation step at pH 6.0 increases the release of M1 and NP into the cytoplasm, whereas a direct exposure of plasma-membrane-bound viruses to pH $\leq$5.5 decreases the release of M1, as well as NP, into the cytoplasm. This might be a result of aggregation of viral M1 and NP that potentially hinders the separation of M1 and vRNPs and transport of NP in the nucleus.

Control experiments were performed in which viruses were preincubated at pH 6.0 with or without amantadine (Fig. 4 *B*): This was done to block the viral M2 channel, thus preventing acidification of the viral interior. Preincubation at pH 6.0 with amantadine resulted in aggregation of M1 and NP upon triggering of fusion at pH 5.0, with a low release of M1 and NP into the cytoplasm. However, aggregation was not observed in the absence of amantadine. We therefore show that preincubating the influenza virus at pH 6.0, simulating endosomal passage, acts on the viral lumen in a way that enables the later release of M1 and NP. In addition, limited proteolysis of recombinant M1 and cryo-electron microscopy of intact virions did not show additional effects of the elevated potassium and calcium concentrations (Figs. S7 and S10) that are apparent during endosomal maturation. This confirms that structural and mechanical changes are mainly induced by the pH drop, potentially enabling efficient infection.

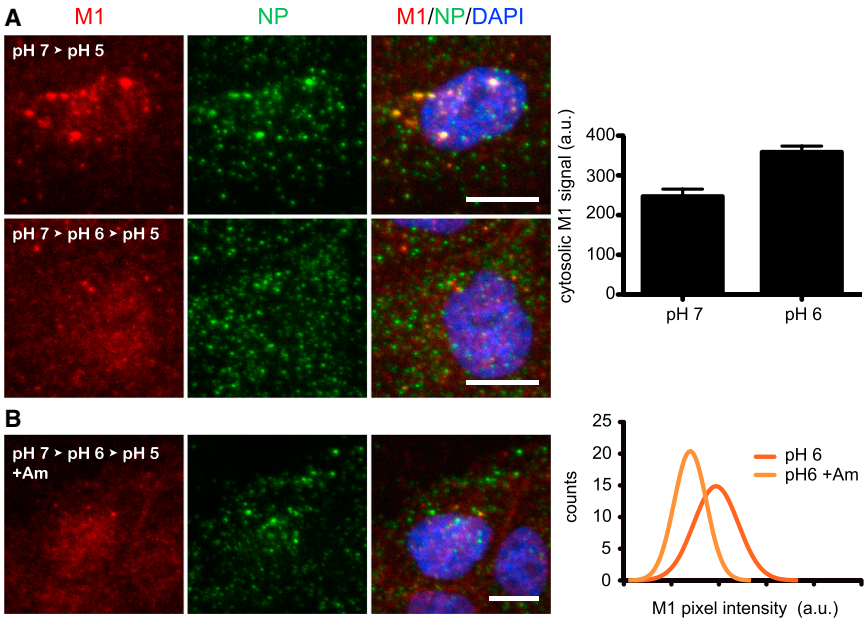

FIGURE 4 Localization of M1 and NP after acid-mediated bypass of virus endocytosis. (*A*) Without preincubation at pH 6.0, both M1 (*upper left*) and NP (*upper center*) were found to be to some extent clustered and colocalized. After preincubation at pH 6.0 (*upper right*), the aggregation decreased and M1 and NP were now more homogenously distributed through the cell. Right: Quantification of cytosolic M1 at the different preincubation conditions. The mean pixel intensity ($\pm$ SE) was measured for equally sized *z*-stacks. Large aggregates were excluded from the selected regions. Scale bar, 10 μm. (*B*) At left, it can be seen that 10 μM amantadine, which blocks the M2-mediated transfer of proton to the viral lumen, yielded a punctate staining after a viral fusion assay at pH 5.0 using a pH 6.0 preincubated sample. This demonstrates that acidification of the viral lumen is essential for the release of M1 and NP into the cytoplasm. At right is a histogram showing that the individual pixel intensity increased upon amantadine treatment as a result of the more punctate staining. Scale bar, 10 μm. To see this figure in color, go online.

Both softening steps are required for efficient infection

To investigate the effect of subacidic pH preincubation on viral infection, influenza A/Panama/2007/99 viruses were incubated at pH 6 or 7 for 30 min and bound to MDCK cells before fusion was triggered using low-pH buffer. Bafilomycin A was added to prevent infection via the endocytotic route. The cells were fixed 5 h after acid bypass and were immunostained against the viral NP. At 5 h postinfection, both normal endocytotic infection and infection after bypass led to a strong NP signal in the nucleus and incipient accumulation of signal in the cytoplasm, as well as to M1 accumulation in the cytoplasm (Fig. S11).

To quantify the number of infected cells, overview images were taken (Fig. 5 *A*) and analyzed using the automated image analysis platform CellProfiler (19) (Figs. 5 *B* and S12). Compared to normal control infection, 13% of the cells were infected after pH 6 preincubation and acid bypass (Fig. S12). As compared to infection via the normal endocytotic route, this reduced infection efficiency could be due to faulty routing of NP to the nucleus in the absence of endosomes or partly inactivated HA and hence reduced fusion. Without the preincubation step, only 5% of the cells were infected after direct fusion (Fig. S12). The addition of amantadine to block intraviral acidification during pH 6 preincubation reduced the infection to the level of pH 7 preincubation.

These results show that subacidic pH preincubation before fusion at pH 5 leads to significantly increased infection efficiency.

DISCUSSION

The endocytotic pathway involves several distinct intermediate compartments differing from others essentially in the degree of their acidification. Our study suggests that influenza virus has optimally adapted to this sequential acidification to ensure efficient genome release. We show here that the uncoating of influenza virus at low pH occurs in two distinct steps that both result in a significant softening of the virions, indicating in each case structural changes in the virus. In addition, a bypass virus-cell fusion assay showed that NP release inside cells, and subsequent nucleus infection, requires both the acidification of the lumen at pH 6.0 and membrane fusion at pH 5.0. We therefore shed light on a two-step mechanism for the uncoating of the influenza virus genome.

Step 1 of virus uncoating. At pH 6.0, the stiffness of influenza virions decreased by 26% (Fig. 2 *A*). The stiffness of bald viruses decreased as well, though to a lower extent. The effect of incubating bald viruses at pH 6.0 was reversed after bringing them back to pH 7. Two contributions to the measured changes could therefore be identified. The most prominent effect originated from spike glycoproteins, and

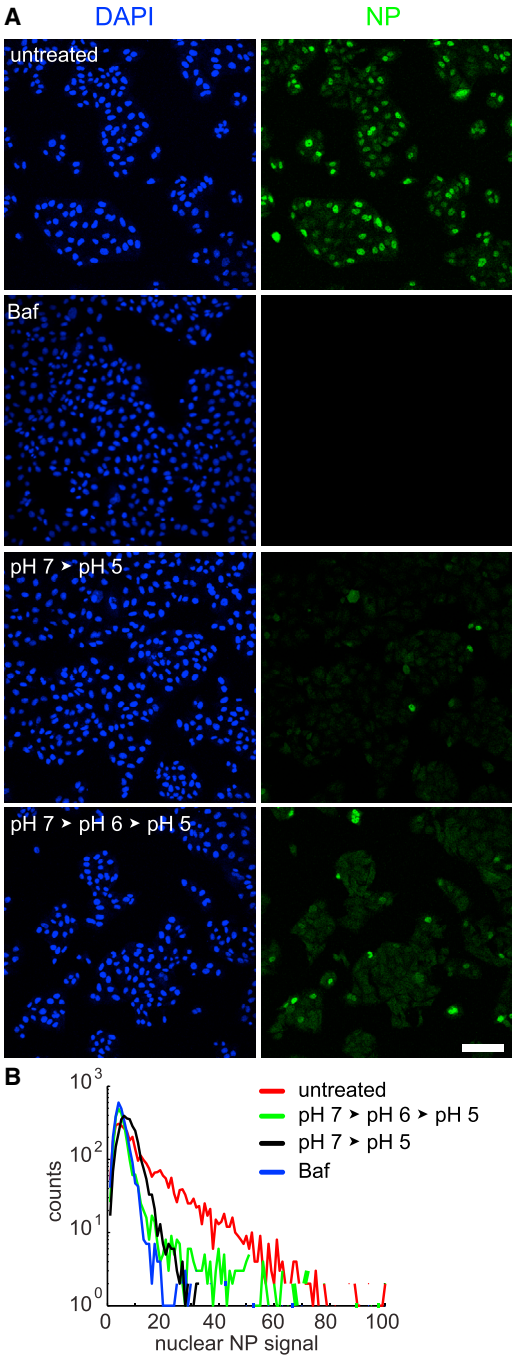

FIGURE 5 Infection efficiency after acid-mediated bypass of virus endocytosis. Influenza viruses were preincubated at the indicated pH conditions and bound to MDCK cells on ice for 10 min before acid-mediated bypass was induced by addition of pH 5 buffer. The cells were incubated for 5 h in infection medium supplemented with 200 nM bafilomycin A, then fixed and immunostained against the viral NP. (*A*) Overview images were taken and analyzed using CellProfiler. (*B*) Histogram of the nuclear NP signal in the respective conditions. The untreated normal infection showed ~60% infected cells. In contrast, an effective block of endocytotic infection could be shown using bafilomycin A treatment (*Baf*). Direct bypass after pH 7 preincubation (pH 7 → pH 5) reduced the infection efficiency to 5% of the control level. A subacidic preincubation at pH 6 before fusion (pH 7 → pH 6 → pH 5) led to 14% infected cells compared to the control level. Scale bar, 100 μm. To see this figure in color, go online.

another, smaller yet significant, effect was attributed to a modification of the viral lumen. It is apparently difficult to reconcile our observation of a spike-dependent softening of the virus at pH 6.0 with the knowledge that influenza HA only undergoes its fusogenic conformational change at lower pH values (Fig. S5 *C*). However, we provide two hypotheses that could explain our measurements.

1. Although HA preserves its prefusion conformation in subacidic conditions, it was shown that its resistance to thermal denaturation is considerably lowered (the difference between the Tm at pH 7 and that at pH 6 was 7°), indicating that its structure at pH 6 is far less compact than at neutral pH (22). Conformational states with low compactness are expected to be more compliant (25).
2. A gain of mobility of HA may also account for this change. A wealth of experimental data supports the idea that an interaction exists between HA and M1 (26). Upon opening of M2 at pH 6 and partial protonation of M1, the HA-M1 interaction could be disrupted, though the M1 layer and the HA conformation apparently remain intact.

Step 2 of virus uncoating. In the second step, from pH 6.0 to pH 5.5, the stiffness decreased by 36% compared to that at pH 7.4. A further lowering of the pH to 5.0 did not significantly soften viruses any further (Fig. 2 *A*). This softening was not reversed by reneutralization of the virus preparation, nor was it related to the fusogenic transconformation of HA. This, along with electron microscopy observations (Fig. 2 *B*), showed us that the second step corresponded to an irreversible dissociation of M1 from the lipid envelope. The irreversibility of this reaction certainly arises from M1 aggregation after dissociation from the viral membrane (2).

Although the origin of the second step thus seems clear, neither mechanical measurements nor electron microscopy could help us identify the cause of the first, reversible, step that occurred above pH 6.0 for bald viruses. Electron microscopy of viruses incubated at pH 6 did not show any significant M1 dissociation from the envelope. Therefore, we must conclude that the acidification of the viral lumen at pH 6.0, triggered by the opening of the M2 proton channel, affects the organization of the interior of the virus in a more subtle way. Along with a possible, yet unseen fragilization of the M1-M1 or M1-HA interaction, the dissociation of vRNP from M1 could also contribute to the first step of viral uncoating: Biochemical characterizations showed that the C-terminal domain of M1 is able to bind the vRNP at neutral pH (27). M1-vRNP complexes may be isolated at neutral pH, but the complex dissociates at acidic pH (28). Moreover, whereas the association of M1 with vRNP in the cytoplasm inhibits their nuclear import, the latter process could be restored by acidifying the cytoplasm to pH 6, indicating that the pH of the early endosome may be sufficient to disrupt the M1-vRNP interaction (5). Contacts are made between the vRNP rods and the M1 layer (29,30). vRNPs also contact the envelope at the budding front, although M1 is absent there. Such contacts may strengthen the shell in a way comparable to that in which DNA was found to reinforce viral protein capsids (10). The apparent absence of a preferential site on the M1 layer where vRNPs can bind could help to explain why the first observed phase was reversible (27,29).

Whichever scenario accounts for our observation of a rearrangement of the influenza virus at step 1, bypass experiments provide evidence that this very step is essential for M1-NP dissociation and hence for efficient infection. Our data indicate that influenza virus needs to be primed in early endosomes to properly release the viral genome from late endosomes: This priming may affect the intermolecular association of various viral building blocks. If the virus did not pass early endosomes, M1 and vRNP would aggregate inside the virus, thus preventing proper genome release. It is interesting that, unlike influenza, other enveloped viruses, such as Semliki Forest Virus or Vesicular Stomatitis Virus (VSV), are able to fuse with early endosomes, and that the pH of the fusogenic conformational changes of the E1 or G (pH 6.2–5.5) is adjusted to meet that requirement. Despite this, it has been observed that VSV does not release its genome directly after membrane fusion, but rather stores its nucleocapsid in the inner membrane of multivesicular bodies until the latter fuse with the limiting membrane of more acidic compartments, later during endosomal transport (31). This might imply a strategy used by the virus to protect its genome during the passage inside the cell, strengthening the suggestion that for efficient infection, viruses such as influenza or VSV release their genome assemblies at the late-endosome stage, and not earlier.

Influenza may have evolved its components to make this targeting possible. The optimum pH for HA fusion activity seems to be adapted to permit fusion only after the viruses have gone through the early-endosome stage (32). The pH at which the M1 layer dissociates lies within the pH range at which fusion occurs. However, cryo-electron tomography shows that if viruses are only subjected to the pH of late endosomes for a short time, a significant amount of M1 remains membrane-bound (2,8) although large amounts of HA have acquired their fusion-mediating conformation (21). One can draw a simple sequential scheme of the steps leading to efficient genome release into the cytoplasm (Fig. 6). First, in early endosomes, the viral lumen gets weakly acidified and undergoes a structural change, with a possible disruption of the M1-vRNP interaction, and/or a fragilization of the M1 layer. This step depends on an active M2 proton channel. Next, as the pH is lowered, dissociation of M1 from the viral bilayer has to proceed in a way that permits the conformational change of HA and, eventually, membrane fusion. These steps have to precede any M1 aggregation at the envelope and accompanying reassociation with vRNPs preventing release of the genome, respectively.

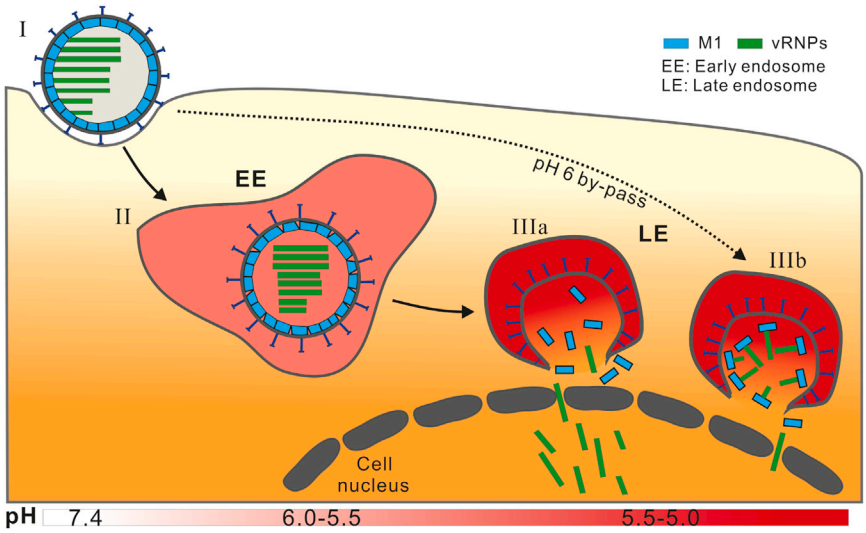

FIGURE 6 Proposed model of the sequential influenza virus uncoating and consequences of bypassing the early endosome. This scheme proposes a sequence for the uncoating of influenza virus. The potential consequences of bypassing early endosomes for genome release are shown more to highlight the importance of sequential endocytotic trafficking for viral unpacking than to explain the bypass assay used in this study. To see this figure in color, go online.

Finally, as HA reaches its full fusion activity, the genome is released into the cytoplasm. We propose that the structural changes of the influenza virus proteins are optimally adapted to the virus journey through the different endosomal maturation stages. This scheme facilitates a sequential uncoating of the virus, of which we have identified two essential steps.

SUPPORTING MATERIAL

Twelve figures, one table, Supporting Materials and Methods, and references (33–42) are available at http://www.biophysj.org/biophysj/supplemental/S0006-3495(14)00224-0.

We are indebted to Sabine Schiller (Humboldt University, Berlin) for technical assistance. We thank Donna and Tom Jovin (MPI-BC, Göttingen) for access to the Zetasizer machine.

S.L., F.E., A.H., and I.A.T.S. designed the research. C.S. purified virus samples and performed fusion and bypass experiments and analysis. F.E. performed additional spectroscopy. S.L. performed AFM experiments. K.L. performed electron microscopy. S.L., F.E., and I.A.T.S. analyzed the AFM data. C.H. and S.C. purified the M1 protein and performed limited proteolysis experiments. S.L., C.S., A.H., F.E., and I.A.T.S wrote the article. The project was supported by the Deutsche Forschungsgemeinschaft (SFB 740 to S.C. and A.H.; HE 3763/15-1 to C.H.; SFB 765 and TP C6 to C.S. and K.L.; SFB 860 to S.L.; and Research Center for Nanoscale Microscopy and Molecular Physiology of the Brain to F.E. and I.A.T.S.).

REFERENCES

1. Skehel, J. J., and D. C. Wiley. 2000. Receptor binding and membrane fusion in virus entry: the influenza hemagglutinin. *Annu. Rev. Biochem.* 69:531–569.
2. Calder, L. J., S. Wasilewski, …, P. B. Rosenthal. 2010. Structural organization of a filamentous influenza A virus. *Proc. Natl. Acad. Sci. USA.* 107:10685–10690.
3. Noda, T., H. Sagara, …, Y. Kawaoka. 2006. Architecture of ribonucleoprotein complexes in influenza A virus particles. *Nature.* 439:490–492.
4. Bui, M., E. G. Wills, …, G. R. Whittaker. 2000. Role of the influenza virus M1 protein in nuclear export of viral ribonucleoproteins. *J. Virol.* 74:1781–1786.
5. Martin, K., and A. Helenius. 1991. Nuclear transport of influenza virus ribonucleoproteins: the viral matrix protein (M1) promotes export and inhibits import. *Cell.* 67:117–130.
6. Sieczkarski, S. B., and G. R. Whittaker. 2003. Differential requirements of Rab5 and Rab7 for endocytosis of influenza and other enveloped viruses. *Traffic.* 4:333–343.
7. Grigoryan, G., D. T. Moore, and W. F. DeGrado. 2011. Transmembrane communication: general principles and lessons from the structure and function of the M2 proton channel, K^+ channels, and integrin receptors. *Annu. Rev. Biochem.* 80:211–237.
8. Fontana, J., G. Cardone, …, A. C. Steven. 2012. Structural changes in Influenza virus at low pH characterized by cryo-electron tomography. *J. Virol.* 86:2919–2929.
9. Chernomordik, L. V., and M. M. Kozlov. 2003. Protein-lipid interplay in fusion and fission of biological membranes. *Annu. Rev. Biochem.* 72:175–207.
10. Carrasco, C., A. Carreira, …, P. J. de Pablo. 2006. DNA-mediated anisotropic mechanical reinforcement of a virus. *Proc. Natl. Acad. Sci. USA.* 103:13706–13711.
11. de Pablo, P. J., I. A. Schaap, …, C. F. Schmidt. 2003. Deformation and collapse of microtubules on the nanometer scale. *Phys. Rev. Lett.* 91:098101.
12. Ivanovska, I. L., P. J. de Pablo, …, G. J. Wuite. 2004. Bacteriophage capsids: tough nanoshells with complex elastic properties. *Proc. Natl. Acad. Sci. USA.* 101:7600–7605.
13. Roos, W. H. 2011. How to perform a nanoindentation experiment on a virus. *Methods Mol. Biol.* 783:251–264.
14. Li, S., F. Eghiaian, …, I. A. Schaap. 2011. Bending and puncturing the influenza lipid envelope. *Biophys. J.* 100:637–645.
15. Schaap, I. A., F. Eghiaian, …, C. Veigel. 2012. Effect of envelope proteins on the mechanical properties of influenza virus. *J. Biol. Chem.* 287:41078–41088.
16. Harris, A., G. Cardone, …, A. C. Steven. 2006. Influenza virus pleiomorphy characterized by cryoelectron tomography. *Proc. Natl. Acad. Sci. USA.* 103:19123–19127.
17. Brand, C. M., and J. J. Skehel. 1972. Crystalline antigen from the influenza virus envelope. *Nat. New Biol.* 238:145–147.
18. Eghiaian, F., and I. A. Schaap. 2011. Structural and dynamic characterization of biochemical processes by atomic force microscopy. *Methods Mol. Biol.* 778:71–95.

19. Carpenter, A. E., T. R. Jones, …, D. M. Sabatini. 2006. CellProfiler: image analysis software for identifying and quantifying cell phenotypes. *Genome Biol.* 7:R100.

20. Carrasco, C., M. Douas, …, P. J. de Pablo. 2009. The capillarity of nanometric water menisci confined inside closed-geometry viral cages. *Proc. Natl. Acad. Sci. USA.* 106:5475–5480.

21. Krumbiegel, M., A. Herrmann, and R. Blumenthal. 1994. Kinetics of the low pH-induced conformational changes and fusogenic activity of influenza hemagglutinin. *Biophys. J.* 67:2355–2360.

22. Remeta, D. P., M. Krumbiegel, …, R. Blumenthal. 2002. Acid-induced changes in thermal stability and fusion activity of influenza hemagglutinin. *Biochemistry.* 41:2044–2054.

23. Lee, K. K. 2010. Architecture of a nascent viral fusion pore. *EMBO J.* 29:1299–1311.

24. Helenius, A., J. Kartenbeck, …, E. Fries. 1980. On the entry of Semliki forest virus into BHK-21 cells. *J. Cell Biol.* 84:404–420.

25. Elms, P. J., J. D. Chodera, …, S. Marqusee. 2012. The molten globule state is unusually deformable under mechanical force. *Proc. Natl. Acad. Sci. USA.* 109:3796–3801.

26. Chen, B. J., G. P. Leser, …, R. A. Lamb. 2007. Influenza virus hemagglutinin and neuraminidase, but not the matrix protein, are required for assembly and budding of plasmid-derived virus-like particles. *J. Virol.* 81:7111–7123.

27. Baudin, F., I. Petit, …, R. W. Ruigrok. 2001. In vitro dissection of the membrane and RNP binding activities of influenza virus M1 protein. *Virology.* 281:102–108.

28. Ye, Z., T. Liu, …, R. A. Levandowski. 1999. Association of influenza virus matrix protein with ribonucleoproteins. *J. Virol.* 73:7467–7473.

29. Fournier, E., V. Moules, …, R. Marquet. 2012. A supramolecular assembly formed by influenza A virus genomic RNA segments. *Nucleic Acids Res.* 40:2197–2209.

30. Noda, T., Y. Sugita, …, Y. Kawaoka. 2012. Three-dimensional analysis of ribonucleoprotein complexes in influenza A virus. *Nat. Commun.* 3:639.

31. Le Blanc, I., P. P. Luyet, …, J. Gruenberg. 2005. Endosome-to-cytosol transport of viral nucleocapsids. *Nat. Cell Biol.* 7:653–664.

32. Korte, T., K. Ludwig, …, A. Herrmann. 1999. Conformational intermediates and fusion activity of influenza virus hemagglutinin. *J. Virol.* 73:4567–4574.

33. Müller, D. J., D. Fotiadis, …, A. Engel. 1999. Electrostatically balanced subnanometer imaging of biological specimens by atomic force microscope. *Biophys. J.* 76:1101–1111.

34. Huang, Q., R. Opitz, …, A. Herrmann. 2002. Protonation and stability of the globular domain of influenza virus hemagglutinin. *Biophys. J.* 82:1050–1058.

35. Rachakonda, P. S., M. Veit, …, A. Herrmann. 2007. The relevance of salt bridges for the stability of the influenza virus hemagglutinin. *FASEB J.* 21:995–1002.

36. Moncelli, M. R., L. Becucci, and R. Guidelli. 1994. The intrinsic pKa values for phosphatidylcholine, phosphatidylethanolamine, and phosphatidylserine in monolayers deposited on mercury electrodes. *Biophys. J.* 66:1969–1980.

37. Reference deleted in proof.

38. van Meer, G., D. R. Voelker, and G. W. Feigenson. 2008. Membrane lipids: where they are and how they behave. *Nat. Rev.* 9:112–124.

39. Reference deleted in proof.

40. Korte, T., and A. Herrmann. 1994. pH-dependent binding of the fluorophore bis-ANS to influenza virus reflects the conformational change of hemagglutinin. *Eur. Biophys. J.* 23:105–113.

41. Arbuzova, A., T. Korte, …, A. Herrmann. 1994. On the validity of lipid dequenching assays for estimating virus fusion kinetics. *Biochim. Biophys. Acta.* 1190:360–366.

42. Schägger, H., and G. von Jagow. 1987. Tricine-sodium dodecyl sulfate-polyacrylamide gel electrophoresis for the separation of proteins in the range from 1 to 100 kDa. *Anal. Biochem.* 166:368–379.